Selective Excitation of Atomic-Scale Dynamics by Coherent Exciton Motion in the Non-Born–Oppenheimer Regime

DATASET · FEBRUARY 2014

1 AUTHOR:

Zhaogang Nie

Nanyang Technological University

38 PUBLICATIONS **341** CITATIONS

SEE PROFILE

THE JOURNAL OF PHYSICAL CHEMISTRY Letters

Letter

pubs.acs.org/JPCL

Selective Excitation of Atomic-Scale Dynamics by Coherent Exciton Motion in the Non-Born−Oppenheimer Regime

Zhaogang Nie,[†] Run Long,[‡,§] Jialin Li,[†] Yi Ying Zheng,[†] Oleg V. Prezhdo,*[,‡] and Zhi-Heng Loh*[,†]

[†]Division of Chemistry and Biological Chemistry, and Division of Physics and Applied Physics, School of Physical and Mathematical Sciences, Nanyang Technological University, Singapore 631371, Singapore

[‡]Department of Chemistry, University of Rochester, RC Box 270216, Rochester, New York 14627, United States

[§]School of Physics, Complex Adaptive Systems Laboratory, University College Dublin, Belfield, Dublin 4, Ireland

Supporting Information

ABSTRACT: Time-domain investigations of the nonadiabatic coupling between electronic and vibrational degrees of freedom have focused primarily on the formation of electronic superpositions induced by atomic motion. The effect of electronic nonstationary-state dynamics on atomic motion remains unexplored. Here, phase-coherent excitation of the two lowest electronic transitions in semiconducting single-walled carbon nanotubes by broadband <5-fs pulses directly triggers coherent exciton motion along the axis of the nanotubes. Optical pump−probe spectroscopy with sub-10-fs time resolution reveals that exciton motion selectively excites the high-frequency G mode coherent phonon, in good agreement with results obtained from time-domain ab initio simulations. This observed phenomenon arises from the direct modulation of the C−C interatomic potential by coherent exciton motion on a time scale that is commensurate with atomic motion. Our results suggest the possibility of employing light-field manipulation of electron densities in the non-Born−Oppenheimer regime to initiate selective atomic motion.

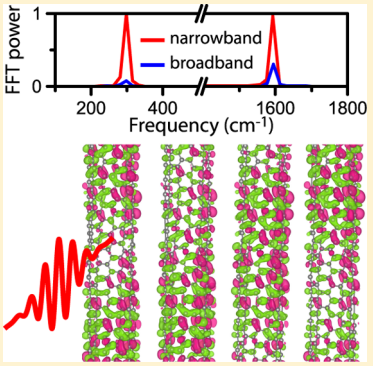

SECTION: Spectroscopy, Photochemistry, and Excited States

The Born−Oppenheimer approximation provides the fundamental framework for understanding a wide variety of physical and chemical phenomena in molecular systems.[1] This approximation is based on the orders-of-magnitude smaller mass of the electron as compared to nuclei, which allows the former to respond instantaneously to the rearrangement of atoms in space. In this adiabatic limit, the multidimensional map of the total electronic energy to the nuclear configuration yields the potential energy surface on which nuclear wave packets propagate and atomic motion results.

When the electronic energy spacing approaches that for vibrational levels, the commensurate pace at which electrons and nuclei move leads to strong vibronic interaction and, subsequently, to the breakdown of the Born−Oppenheimer approximation.[2] Strong vibronic coupling has been elucidated in systems ranging from simple molecular ions[3] to extended materials such as graphene[4] and single-walled carbon nanotubes (SWNTs).[5,6] Moreover numerous investigations by femtosecond time-resolved spectroscopy and theoretical simulations have established that the ultrafast nonradiative deactivation of molecular excited states originates from non-Born−Oppenheimer dynamics at conical intersections.[7,8] The results of these studies can be rationalized in terms of the nonadiabatic coupling of multiple electronic states by atomic motion.

The recent advent of attosecond time-resolved spectroscopy offers the possibility of investigating ultrafast nonadiabatic quantum dynamics on time scales that are commensurate with electron motion.[9,10] A recent experiment employed attosecond soft X-ray absorption to directly observe valence electron motion in krypton ions produced by strong-field ionization.[11] Going beyond atoms to molecules and extended systems requires an in-depth understanding of how coherent electron motion influences the propagation of vibrational wave packets and vice versa. SWNTs are prime candidates for such studies because their defect-free structures, high carrier mobilities, and exquisite performances as field-effect transistors position them at the forefront of molecular nanoelectronics[12,13] and photovoltaics[14,15] research. Here, we employ optical pump−probe spectroscopy with few-cycle (<5 fs) laser pulses to show that driving coherent exciton motion in semiconducting SWNTs triggers vibrational mode-selective atomic-scale dynamics that result from the breakdown of the Born−Oppenheimer approximation. It is important to note that the sub-10-fs time resolution of our experimental apparatus prevents the direct observation of exciton motion, which is expected to occur on few-femtosecond time scales. Nevertheless, our experimental results provide clear evidence for the effect of coherent electronic excitation on the spectral and phase characteristics of

Received: September 10, 2013
Accepted: November 26, 2013

   dx.doi.org/10.1021/jz401945m | J. Phys. Chem. Lett. 2013, 4, 4260−4266

the coherent phonons, enabled by the nonadiabatic coupling between the electronic and vibrational degrees of freedom.

The valence electronic structure of SWNTs consists of van Hove singularities and Wannier–Mott excitons.[16] The former are associated with the one-dimensional quantum confinement of carriers, whereas the latter arise from many-body effects and correspond to eigenstates that are accessed by resonant optical transitions from the ground state.[17] The spectral bandwidth of the <5-fs few-cycle laser pulses used in our experiments is sufficiently broad (~570–950 nm at −10 dB spectral intensity) to simultaneously excite the E_{11} and E_{22} transitions of semiconducting SWNTs (Figure 1a), where E_{nn} denotes the

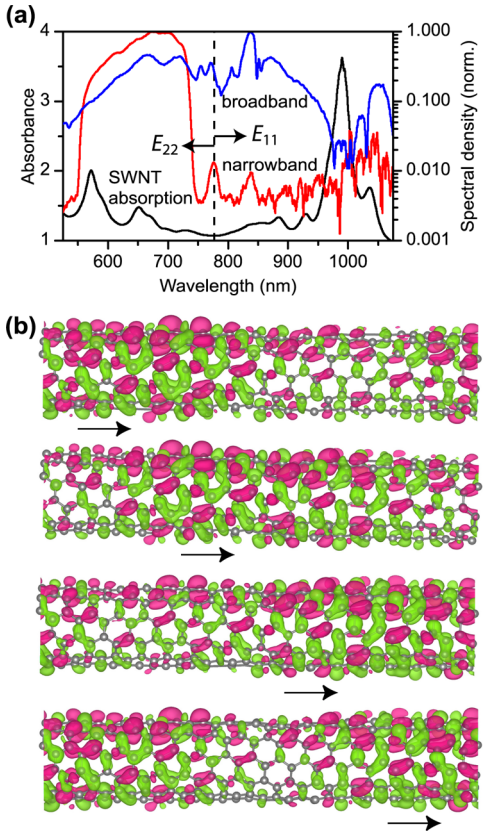

Figure 1. (a) Optical absorption spectrum (black line) of the SWNT thin film sample, showing spectral regions that correspond to the E_{11} and E_{22} transitions. The spectral densities of the few-cycle pulse used for coherent broadband excitation (blue line) and the narrowband pulse used for selective E_{22} excitation (red line) are also shown. (b) Visualization of exciton motion in a (6,5) carbon nanotube resulting from the coherent excitation of the E_{11} and E_{22} transitions, as obtained from time-domain density functional theory calculations. The plots show the transition densities, in which red (green) contours represent the accumulation of electron (hole) density relative to the ground state. The time lapse between successive plots is $T_{el}/4 \approx 1$ fs. The arrows denote the direction of coherent excitonic motion.

excitonic state that is associated with the nth van Hove singularity in the valence/conduction band. Such an electronic superposition sets forth coherent exciton motion—the correlated motion of bound electron–hole pairs—along the SWNT axis (Figure 1b), in sharp contrast to the stationary states produced following selective excitation of either the E_{11} or E_{22} transition. An estimate for the time scale for exciton motion is obtained from the relation $T_{el} = h/\Delta E$, where T_{el} is the oscillation period obtained from the Bohr frequency condition for the excitonic superposition, h is Planck's constant, and ΔE is the energy separation between the E_{22} and E_{11} excitonic states. (Note that dissimilar exciton binding energies of the E_{22} and E_{11} states[18] would necessitate consideration of excitonic energy differences in the estimate of T_{el}, rather than single-particle energy differences.) For <1-nm-diameter semiconducting SWNTs, the electronic oscillation period is expected to be ~4–8 fs. It is important to note that these time scales should be regarded as approximate, given that the atoms are assumed to be frozen in the above calculation. In fact, our results show that strong nonadiabatic coupling exists between electron motion in a SWNT and its nuclear degrees of freedom.

Following broadband excitation by few-cycle laser pulses, the time-evolution of the differential transmission ($\Delta T/T$) spectrum (Figure 2a) exhibits ground-state bleaching and stimulated emission from the excited states. At a probe wavelength of 680 nm, where absorption by the (8,3) nanotube is dominant, the biphasic recovery time constants are 38 ± 1 fs and 0.67 ± 0.01 ps. The fast time constant is in agreement with that previously assigned to intersubband relaxation from the E_{22} to the E_{11} state, whereas the slow time constant is attributed to subsequent relaxation from E_{11} to the ground state.[19] (In addition to stimulated emission from E_{22}, note that probing at the E_{22} transition also reveals the dynamics of ground-state bleaching and is therefore sensitive to electronic relaxation of E_{11} to the ground state.) Pronounced modulations with a 21-fs period are observed across the majority of the probe spectral range, as confirmed by the presence of a dominant frequency at 1590 cm^{-1} in the 2D FFT power spectrum (Figure 2b). This oscillation is attributed to the G mode longitudinal optical (LO) phonon.[20] Its observation in the time domain arises from the photoinduced generation of a coherent phonon, that is, the collective stretching motion of C–C double bonds along the axis of the SWNT. Aside from the G mode phonon, the coherent radial breathing mode (RBM) phonon[20] at ~300 cm^{-1} shows up prominently at 660 nm. The above results, which are obtained from the coherent photoexcitation of the E_{11} and E_{22} states with broadband few-cycle pulses, should be contrasted with those in which only the E_{22} state is excited. Multiple reflections of the few-cycle pulse off of a visible dielectric mirror pair followed by additional dispersion compensation furnish a relatively narrowband (560–737 nm at −10 dB), chirp-free pulse that is a replica of the broadband pulse in the visible (Figure 1a). This narrowband pulse is employed for the selective excitation of the E_{22} state. The time-resolved $\Delta T/T$ spectra and 2D FFT power spectrum obtained with E_{22} excitation are shown in Figure 2c and d, respectively.

The 2D FFT power spectrum recorded with narrowband excitation (Figure 2d) is similar to those previously measured with sub-10-fs visible pump pulses, which access only the E_{22} state.[21,22] Comparison with the 2D FFT power spectrum obtained from broadband excitation reveals qualitative differences, most notably in the wavelength dependence of the G mode power. The G mode FFT power profile shows, in the case of broadband excitation, maxima at probe wavelengths of 567, 592, and 680 nm, which closely coincide with the E_{22} absorption maxima of the (6,5), (6,4), and (8,3) SWNTs, respectively (Figure 2e). In contrast, minima exist at these probe wavelengths with narrowband excitation, in agreement with the previous results obtained from selective access to the E_{22} state.[21] Aside from a change in the G mode FFT power profile, the experimental data also indicate that broadband

dx.doi.org/10.1021/jz401945m | J. Phys. Chem. Lett. 2013, 4, 4260–4266

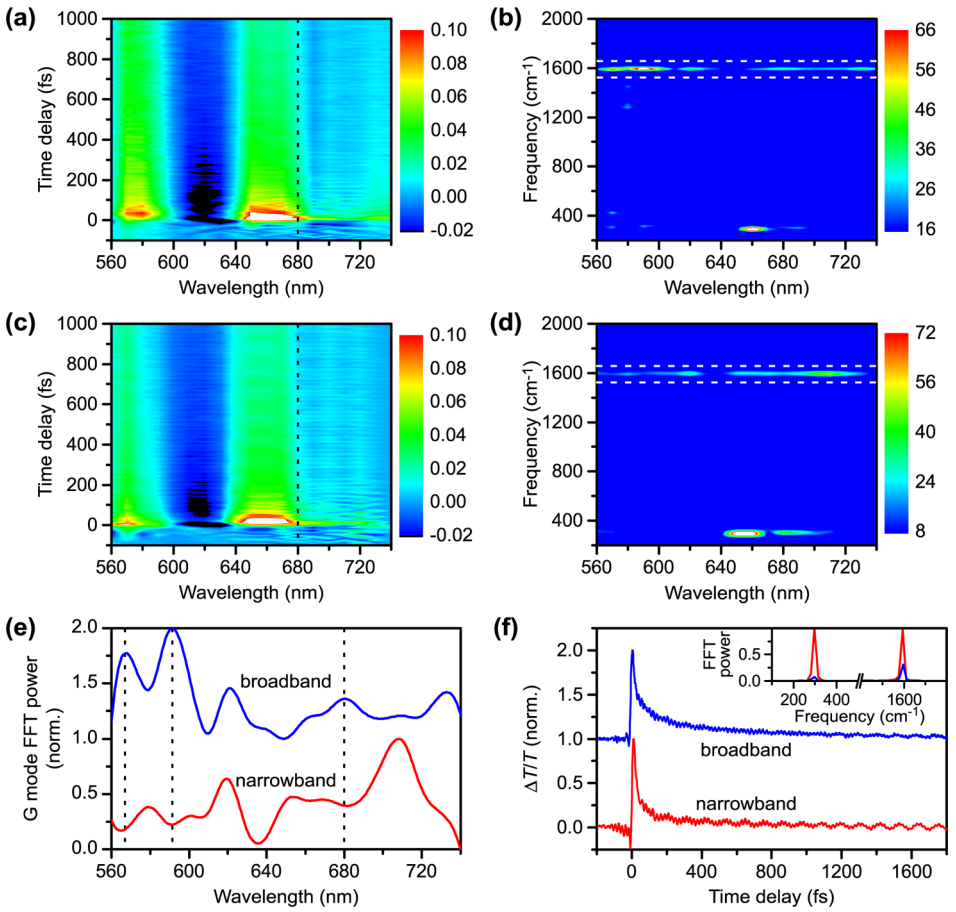

Figure 2. (a) Contour plot of the time-resolved differential transmission spectra and (b) 2D FFT power spectrum obtained with broadband excitation. (c) Contour plot of the time-resolved differential transmission spectra and (d) 2D FFT power spectrum obtained with narrowband E_{22} excitation. The vertical scales for the $\Delta T/T$ signal and the coherent phonon FFT power (in arbitrary units) are provided. (e) Normalized FFT power profiles of the G mode at 1590 cm^{-1} (see the region bounded by dotted lines in b and d) obtained with narrowband (red line) and broadband (blue line) excitation (offset for clarity). The dotted lines indicate positions in the vicinity of the nanotube electronic absorption maxima at which the broadband and narrowband G mode powers are anticorrelated. (f) Differential transmission measured at a 680 nm probe wavelength (see the dotted lines in a and c) for narrowband (red line) and broadband (blue line) excitation (offset for clarity). The FFT power spectra are shown in the inset; both spectra are rescaled such that the RBM power of the narrowband excitation time trace is normalized. Note that the suppression of the RBM oscillation (~110 fs period, 300 cm^{-1} frequency) with broadband excitation is apparent in both the time trace and the FFT power spectrum (see the inset).

coherent excitation results in a significant suppression of the RBM coherent phonon. This effect is easily discernible from the pump−probe time traces collected at a probe wavelength of 680 nm (Figure 2f), where a previous RBM coherent phonon study shows that the (8,3) SWNT response is dominant.[22] The corresponding FFT power spectra, after adjustment to yield the same initial total excited-state population, reveal a 13-fold suppression in the RBM phonon with broadband coherent excitation, whereas the G mode power is only reduced by a factor of 3. Furthermore, a time-domain analysis shows that the cosinusoidal phase of the G mode vibration (ϕ_G) shifts from $(0.50 \pm 0.02)\pi$ to $-(0.10 \pm 0.03)\pi$ upon going from narrowband to broadband excitation (see the Supporting Information), even though the phases of the RBM (ϕ_{RBM}) remain unchanged, [$(0.39 \pm 0.02)\pi$ for narrowband and $(0.38 \pm 0.04)\pi$ for broadband].

The appearance of peaks in the G mode FFT power profile that correspond to the absorption maxima of the (6,5), (6,4), and (8,3) SWNTs (Figure 2e) strongly suggests the involvement of excitonic coherences in coherent phonon generation by the broadband excitation pulse. Indeed, these nanotubes possess E_{11} and E_{22} transitions that lie within the spectral bandwidth of the few-cycle laser pulse, thereby enabling the pump pulse to drive coherent exciton motion. The survival of coherent phonons beyond the lifetimes of the electronically excited states is supported by a multilevel formulation of Redfield relaxation theory.[23] A coherent excitonic origin for the G mode phonon is further substantiated by the wave packet theory of spectrally resolved transient absorption spectroscopy[24] and its recent application[25] to analyzing the results of an attosecond soft X-ray transient absorption experiment.[11] Both analyses show that signatures of exciton motion in the time domain can be found at the maxima of electronic transient absorption spectra, as is observed here in the case of broadband excitation. In contrast, the G mode FFT power profile obtained with narrowband E_{22} excitation reveals minima at the absorption maxima positions, in agreement with the previously established mechanisms for coherent phonon generation involving displacive excitation and/or resonant impulsive stimulated Raman pumping in the electronic ground state.[21,26−28]

dx.doi.org/10.1021/jz401945m | J. Phys. Chem. Lett. 2013, 4, 4260−4266

The phases for the RBM and G mode vibrations retrieved from the time traces measured at 680 nm (Figure 2f) further reveal the unusual manner in which the latter is generated with broadband excitation. First, it should be noted that for a cosinusoidal oscillation in the $\Delta T/T$ signal probed below a resonance, the negative slope that is associated with $\phi_{RBM} \approx 0.4\pi$ implies an initial expansion of the nanotube diameter in response to photoexcitation. In the case of narrowband E_{22} excitation, this outcome is in accord with the previous experimental[29] and theoretical[30] results. The similar ϕ_{RBM} value obtained with broadband excitation can be understood based on the predicted dominant contribution of the E_{22} component to the RBM response when both E_{11} and E_{22} are simultaneously populated by a few-cycle laser pulse.[30] Second, it is found that narrowband excitation yields similar ϕ_{RBM} and ϕ_G values. This result is consistent with the adiabatic following of the RBM motion by the G mode phonon.[26] Finally, in contrast to the similar ϕ_{RBM} values obtained with narrowband and broadband photoexcitation, the G mode vibration exhibits a phase difference of 0.6π between the two excitation regimes. In the spirit of treating photoinduced coherent phonons as driven harmonic oscillators,[30] the -0.6π phase shift observed with broadband photoexcitation is reminiscent of a phase lag that is present when an oscillator is driven nonadiabatically at frequencies higher than its resonance frequency. A possible candidate for this coherent phonon driving term is coherent exciton motion, which in the case of the (8,3) SWNT, occurs on a time scale ($T_{el} \approx 7.4$ fs) that is ~3× shorter than that of the G mode period. It is noteworthy that the odd integer-multiple relation between T_{el} and the 21-fs G mode period minimizes the phase mismatch between the optically induced exciton motion and the subsequent coherent phonon oscillation because the exciton and vibrational motions will have the same phase at every half cycle of the vibrational oscillation. On the other hand, for an even integer-multiple relation between T_{el} and the G mode period, as in the case of the (7,5) and (9,1) nanotubes, the exciton and vibrational motions become out of phase after every full cycle of the vibrational oscillation.

Time-domain ab initio simulations that incorporate electron−phonon coupling[31] are performed to elucidate the manner in which a coherent excitonic superposition selectively drives the G mode coherent phonon. For the (6,5) nanotube, trajectories of the E_{11} and E_{22} transition energies calculated within the single-particle picture exhibit oscillations at both the RBM and G mode frequencies (Figure 3a). These oscillations originate from energy modulations of the van Hove singularities induced by atomic motion. By themselves, the E_{11} and E_{22} states exhibit strong electron−phonon coupling to the RBM (Figure 3b). Furthermore, in agreement with the oppositely signed RBM displacement vectors predicted for the E_{11} and E_{22} transitions,[30] the energy oscillations at the RBM frequency are found to occur in phase for the two transitions such that the RBM is suppressed by $>10^3$-fold in the trajectory for the energy difference $\Delta E = E_{22} - E_{11}$. This energy difference represents the coherent excitonic superposition. The slightly out-of-phase G mode oscillations observed for the individual E_{11} and E_{22} trajectories, on the other hand, result in only a slight decrease in the G mode FFT power of the ΔE trajectory. The net result is a $>10^2$-fold increase in the ratio of the G mode to RBM FFT power upon going from narrowband to broadband excitation. It is therefore the concomitant propagation of nuclear wave packets on both E_{11} and E_{22} states—a distinctly non-Born−Oppenheimer phenomenon—that is responsible for the dominant G mode vibration observed in the case of broadband excitation and whose description necessitates the nonadiabatic dynamical calculations employed here. Intuitively, an electronic superposition that possesses more nodes in its electron density distribution is expected to couple more favorably to higher-frequency phonons.

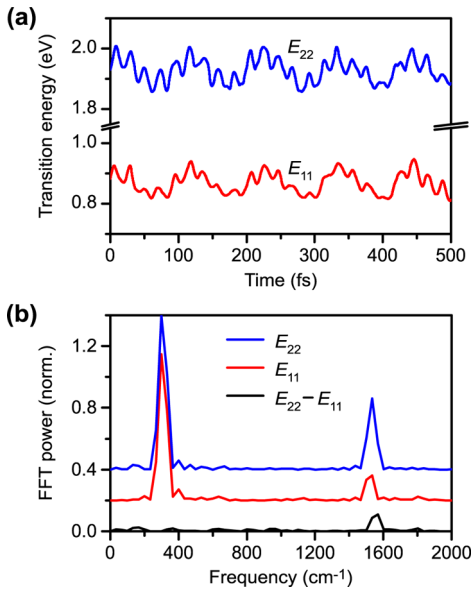

Figure 3. (a) E_{11} and E_{22} transition energies for a (6,5) nanotube obtained from time-domain ab initio calculations. (b) FFT power spectra for the E_{11} (red line), E_{22} (blue line), and ΔE (black line) trajectories, showing selective excitation of the G mode by the coherent superposition. The FFT powers are normalized to that of the RBM mode in the E_{22} trajectory. The FFT power spectra for the E_{11} and E_{22} trajectories are offset by 0.2 and 0.4 units, respectively.

The initiation of coherent phonons by the simultaneous propagation of vibrational wave packets on both the E_{11} and E_{22} states should be contrasted with the previously established displacive and impulsive stimulated Raman excitation mechanisms for coherent phonon generation,[21,22,26−28] both of which involve the propagation of vibrational wave packets on only a single potential energy surface. In this work, the use of near-transform-limited, <5-fs excitation pulses suppresses the impulsive stimulated Raman excitation of the G mode coherent phonon because the short pulse duration prevents appreciable motion of the vibrational wave packet in the excited state before it is coupled back to the ground state.[32] Furthermore, beyond the conventional displacive excitation of vibrational wave packets on a single electronically excited state,[33] the phase-coherent excitation of multiple excitonic states dictates the need to consider the displacive excitation of vibrational wave packets on both E_{11} and E_{22} states. By definition, the involvement of multiple excitonic states in vibrational motion constitutes non-Born−Oppenheimer behavior. The need for a non-Born−Oppenheimer description becomes evident when one realizes that the description of vibrational wave packet motion along a single adiabatic potential energy surface omits coherent excitonic motion, whereas a purely electronic description fails to capture the vibrational motion. Nevertheless, an intuitive, time-domain perspective of the interaction between excitonic and nuclear degrees of freedom in SWNTs can be described as follows. Phase-coherent excitation of the E_{11} and E_{22} states by a broadband, few-cycle laser pulse triggers

dx.doi.org/10.1021/jz401945m | J. Phys. Chem. Lett. 2013, 4, 4260−4266

nonstationary exciton motion along the axis of the nanotube. Oscillation of the charge density along the nanotube with period T_{el} directly modulates the C−C interatomic potential, which in turn sets off the G mode coherent phonon. Because the G mode oscillation period is comparable to the time scale on which the potential energy for the C−C bond is altered, coherent exciton motion can effectively drive the G mode coherent phonon in a manner that is analogous to an electromechanical resonator.

The initiation of coherent atomic-scale dynamics by electron motion differs from the situation encountered in conventional non-Born−Oppenheimer dynamics, in which atomic motion drives the formation of an electronic superposition. These results suggest that studies of coherent electron dynamics, which involve times scales ranging from the attosecond to those that characterize relatively slow intermolecular electronic coherences,[34] will be greatly enriched by the mode-selective generation of vibrational wave packets in the manner observed here. The ability to electronically steer atomic motion on the ∼10-fs time scale paves way for the realization of nanoscale electromechanical systems, such as those based on SWNTs,[35] that can operate at optical frequencies, and also bears promise for the study and control of ultrafast chemical reaction dynamics[36,37] by the direct manipulation of valence electron densities in real time.[38,39]

EXPERIMENTAL AND THEORETICAL METHODS

Few-cycle laser pulses of <5-fs duration with wavelength spanning ∼570−950 nm (at −10 dB spectral intensity) are produced by spectral broadening of the 25-fs output from an amplified Ti:sapphire laser system in a helium-filled hollow-core fiber followed by chirped mirror compression (see the Supporting Information for details). While the E_{11} and E_{22} transitions of SWNTs are located close to the wings of the hollow-core fiber output spectrum, the spectral densities in those regions are nevertheless sufficiently high to enable efficient excitation of these transitions. This is evident from the sizable peak $\Delta T/T$ signal of 0.07 at 572 nm, where the (6,5) nanotube absorbs and where the laser spectral density is ∼10× weaker than that at the maximum. Optical pump−probe measurements are performed with a Mach−Zehnder interferometer, which consists of a motorized translation stage incorporated into the probe arm to generate a computer-controlled time delay between pump and probe pulses. These measurements yield the normalized differential transmission signal, $\Delta T/T = (T_{on} - T_{off})/T_{off}$, where T_{on} (T_{off}) refers to the sample transmission in the presence (absence) of the excitation pump. Typical pulse energies for the pump and probe beams are 160 and 20 nJ, respectively; both beams have focal spot diameters ($1/e^2$) of ∼250 μm. Fluence dependence studies confirm that the transient absorption signal is far from saturated because it remains linear to at least three times the pulse energies used in the experiments. Hence, the effects of phase-space filling, exciton−exciton scattering, and other nonlinear effects that occur at higher pump fluences can safely be neglected.[40,41] The probe beam that is transmitted through the sample is spectrally dispersed in a spectrograph and detected by a photodiode that is connected to a lock-in amplifier. Spectrally resolved measurements allow dynamics that originate from the different SWNT chiralities present in the sample to be disentangled (see the Supporting Information). Retrieval of the initial phase of the coherent phonon signal via time-domain analysis places stringent requirements on the accuracy of the time zero, particularly for the case of the G mode coherent phonon. In our experimental setup, time zero is determined to <1-fs accuracy by cross-correlation of the pump and probe pulses in a 10-μm-thick beta barium borate (BBO) crystal that is located at the sample position. Fitting the measured time traces to a convolution of the sample response with the instrument response function provides an independent check of the accuracy of the zero time delay (see the Supporting Information).

The experiments employ semiconducting SWNTs prepared by the CoMoCat method[42] and dispersed onto a 0.5-mm-thick fused silica substrate. Atomic force microscopy measurements show that the nanotubes have typical lengths of ∼330 ± 160 nm and diameters of ∼1 nm.[22] The high quality of the sample is evident from the Raman spectrum collected with 514.5-nm excitation, which shows a disorder-induced D-band to G-mode intensity ratio of only 0.025 (see the Supporting Information). This intensity ratio suggests graphitic crystallite lengths of >150 nm that are comparable to the typical lengths of the SWNTs. Moreover, because the tube lengths are approximately 2 orders of magnitude larger than the typical few-nanometer size of the Wannier−Mott exciton,[43] complications of the experimental results by tube-end defects are expected to be negligible. The optical absorption spectrum of the sample shows that it is comprised mainly of semiconducting (6,5), (6,4), (8,3), (7,5), and (9,1) nanotubes. Ultrafast dynamics that are dominated by a given nanotube chirality can be extracted by combining the spectrally dispersed differential absorption detection scheme with the judicious choice of probe wavelength. For example, the response from the (8,3) nanotube probed at 680 nm is >10× stronger than the responses from the neighboring (7,5) and (9,1) nanotubes. Furthermore, contributions to the transient absorption signal by metallic SWNTs are expected to be insignificant because the E_{11}^{M} transitions of the ∼1 nm diameter metallic nanotubes that are produced by the CoMoCat method are located at wavelengths shorter than 540 nm,[44] beyond the range of the laser spectrum employed in this work.

We consider the (6,5) nanotube as an example to compute its electronic structure, electron−phonon coupling, and photo-induced electron−phonon dynamics. Our choice of the (6,5) nanotube is motivated by the availability of numerous experimental results that have been obtained on this particular SWNT species. Its unit cell is smaller than, for instance, that of the (8,3) tube, facilitating the calculations. The simulations are carried out using the Vienna ab initio simulation package (VASP).[45] The nonlocal exchange and electron correlation energies are treated with the Perdew−Burke−Ernzerhof (PBE) functional,[46] which is based on the generalized gradient approximation (GGA). The projector augmented wave (PAW) approach is used to describe the interaction of the ionic cores with the valence electrons.[47] To prevent spurious interactions between the images, 5 Å of vacuum is added in the direction perpendicular to the axis of the tube in the periodic cell. The structure of the nanotube and the dimension of the simulation cell along the tube are optimized to obtain the minimum-energy structure. After heating the system to 300 K by repeated velocity rescaling, a 1-ps microcanonical trajectory is run in the ground electronic state with a 1-fs time step. Then, superpositions of E_{11} and E_{22} transitions are excited at randomly chosen points along the trajectories, mimicking the broadband excitation, and the ensuing nonadiabatic dynamics are followed using time-domain density functional theory, as described in ref 48.

dx.doi.org/10.1021/jz401945m | J. Phys. Chem. Lett. 2013, 4, 4260−4266

■ ASSOCIATED CONTENT

Supporting Information

Additional information is provided on (1) the generation and characterization of few-cycle optical pulses and their implementation in optical pump−probe spectroscopy, (2) the assignment of the transitions observed in the optical absorption spectrum to the various chiralities present in the SWNT sample and the calculation of the absorbed laser spectrum by the E_{11} and E_{22} transitions of the (8,3) SWNT, (3) the Raman spectrum of the SWNT sample, (4) the time-domain analysis of the differential transmission time traces obtained with broadband and narrowband excitation, and (5) the results for G mode coherent phonon generation observed at the E_{11} transition following broadband and narrowband excitation. This material is available free of charge via the Internet at http://pubs.acs.org.

■ AUTHOR INFORMATION

Corresponding Authors

*E-mail: oleg.prezhdo@rochester.edu (O.V.P.).
*E-mail: zhiheng@ntu.edu.sg (Z.-H.L).

Notes

The authors declare no competing financial interest.

■ ACKNOWLEDGMENTS

This work is supported by a NTU start-up grant, the A*Star Science and Engineering Research Council Public Sector Funding (122-PSF-0011), and the award of a Nanyang Assistant Professorship to Z.-H.L. R.L. thanks the Science Foundation Ireland SIRG Program (11/SIRG/E2172). O.V.P. acknowledges financial support from the U.S. National Science Foundation (CHE-1300118).

■ REFERENCES

(1) Born, M.; Oppenheimer, J. R. Zur Quantentheorie de Molekeln. *Ann. Phys.* **1927**, *84*, 457−484.
(2) Yarkony, D. R. Conical Intersections: The New Conventional Wisdom. *J. Phys. Chem. A* **2001**, *105*, 6277−6293.
(3) Köppel, H.; Cederbaum, L. S.; Domcke, W.; Shaik, S. S. Symmetry Breaking and Non-Born−Oppenheimer Effects in Radical Cations. *Angew. Chem., Int. Ed. Engl.* **1983**, *22*, 210−224.
(4) Pisana, S.; Lazzeri, M.; Casiraghi, C.; Novoselov, K. S.; Geim, A. K.; Ferrari, A. C.; Mauri, F. Breakdown of the Adiabatic Born−Oppenheimer Approximation in Graphene. *Nat. Mater.* **2007**, *6*, 198−201.
(5) Bushmaker, A. W.; Deshpande, V. V.; Hsieh, S.; Bockrath, M. W.; Cronin, S. B. Direct Observation of Born−Oppenheimer Approximation Breakdown in Carbon Nanotubes. *Nano Lett.* **2009**, *9*, 607−611.
(6) Duque, J. G.; Chen, H.; Swan, A. K.; Shreve, A. P.; Kilina, S.; Tretiak, S.; Tu, X.; Zheng, M.; Doorn, S. K. Violation of the Condon Approximation in Semiconducting Carbon Nanotubes. *ACS Nano* **2011**, *5*, 5233−5241.
(7) Polli, D.; Altoè, P.; Weingart, O.; Spillane, K. M.; Manzoni, C.; Brida, D.; Tomasello, G.; Orlandi, G.; Kukura, P.; Mathies, R. A.; et al. Conical Intersection Dynamics of the Primary Photoisomerization Event in Vision. *Nature* **2010**, *467*, 440−443.
(8) Gustavsson, T.; Improta, R.; Markovitsi, D. DNA/RNA: Building Blocks of Life under UV Irradiation. *J. Phys. Chem. Lett.* **2010**, *1*, 2025−2030.
(9) Kling, M. F.; Vrakking, M. J. J. Attosecond Electron Dynamics. *Annu. Rev. Phys. Chem.* **2008**, *59*, 463−492.
(10) Krausz, F.; Ivanov, M. Attosecond Physics. *Rev. Mod. Phys.* **2009**, *81*, 163−234.
(11) Goulielmakis, E.; Loh, Z.-H.; Wirth, A.; Santra, R.; Rohringer, N.; Yakovlev, V. S.; Zherebtsov, S.; Pfeifer, T.; Azzeer, A. M.; Kling, M. F.; et al. Real-Time Observation of Valence Electron Motion. *Nature* **2010**, *466*, 739−744.
(12) Tans, S. J.; Verschueren, A. R. M.; Dekker, C. Room-Temperature Transistor Based on a Single Carbon Nanotube. *Nature* **1998**, *393*, 49−52.
(13) Avouris, P.; Chen, Z.; Perebeinos, V. Carbon-Based Electronics. *Nat. Nanotechnol.* **2007**, *2*, 605−615.
(14) Hasobe, T.; Fukuzumi, S.; Kamat, P. V. Organized Assemblies of Single Wall Carbon Nanotubes and Porphyrinr for Photochemical Solar Cells: Charge Injection from Excited Porphyrin into Single-Walled Carbon Nanotubes. *J. Phys. Chem. B* **2006**, *110*, 25477−25484.
(15) D'Souza, F.; Sandanayaka, A. S. D.; Ito, O. SWNT-Based Supramolecular Nanoarchitectures with Photosensitizing Donor and Acceptor Molecules. *J. Phys. Chem. Lett.* **2010**, *1*, 2586−2593.
(16) Dresselhaus, M. S.; Dresselhaus, G.; Saito, R.; Jorio, A. Exciton Photophysics of Carbon Nanotubes. *Annu. Rev. Phys. Chem.* **2007**, *58*, 719−747.
(17) Wang, F.; Dukovic, G.; Brus, L. E.; Heinz, T. F. The Optical Resonances in Carbon Nanotubes Arise from Excitons. *Science* **2005**, *308*, 838−841.
(18) Capaz, R. B.; Spataru, C. D.; Ismail-Beigi, S.; Louie, S. G. Diameter and Chirality Dependence of Exciton Properties in Carbon Nanotubes. *Phys. Rev. B* **2006**, *74*, 121401.
(19) Manzoni, C.; Gambetta, A.; Menna, E.; Meneghetti, M.; Lanzani, G.; Cerullo, G. Intersubband Exciton Relaxation Dynamics in Single-Walled Carbon Nanotubes. *Phys. Rev. Lett.* **2005**, *94*, 207401.
(20) Dresselhaus, M. S.; Dresselhaus, G.; Saito, R.; Jorio, A. Raman Spectroscopy of Carbon Nanotubes. *Phys. Rep.* **2005**, *409*, 47−99.
(21) Lüer, L.; Gadermaier, C.; Crochet, J.; Hertel, T.; Brida, D.; Lanzani, G. Coherent Phonon Dynamics in Semiconducting Carbon Nanotubes: A Quantitative Study of Electron−Phonon Coupling. *Phys. Rev. Lett.* **2009**, *102*, 127401.
(22) Kobayashi, T.; Nie, Z.; Du, J.; Okamura, K.; Kataura, H.; Sakakibara, Y.; Miyata, Y. Electronic Relaxation and Coherent Phonon Dynamics in Semiconducting Single-Walled Carbon Nanotubes with Several Chiralities. *Phys. Rev. B* **2013**, *88*, 035424.
(23) Jean, J. M.; Fleming, G. R. Competition Between Energy and Phase Relaxation in Electronic Curve Crossing Processes. *J. Chem. Phys.* **1995**, *103*, 2092−2101.
(24) Pollard, W. T.; Lee, S.-Y.; Mathies, R. A. Wave Packet Theory of Dynamic Absorption Spectra in Femtosecond Pump−Probe Experiments. *J. Chem. Phys.* **1990**, *92*, 4012−4029.
(25) Santra, R.; Yakovlev, V. S.; Pfeifer, T.; Loh, Z.-H. Theory of Attosecond Transient Absorption Spectroscopy of Strong-Field-Generated Ions. *Phys. Rev. A* **2011**, *83*, 033405.
(26) Lim, Y.-S.; Yee, K.-J.; Kim, J.-H.; Hároz, E. H.; Shaver, J.; Kono, J.; Doorn, S. K.; Hauge, R. H.; Smalley, R. E. Coherent Latice Vibrations in Single-Walled Carbon Nanotubes. *Nano Lett.* **2006**, *6*, 2696−2700.
(27) Gambetta, A.; Manzoni, C.; Menna, E.; Meneghetti, M.; Cerullo, G.; Lanzani, G.; Tretiak, S.; Piryatinski, A.; Saxena, A.; Martin, R. L. Real-Time Observation of Nonlinear Coherent Phonon Dynamics in Single-Walled Carbon Nanotubes. *Nat. Phys.* **2006**, *2*, 515−520.
(28) Graham, M. W.; Calhoun, T. R.; Green, A. A.; Hersam, M. C.; Fleming, G. R. Two-Dimensional Electronic Spectroscopy Reveals the Dynamics of Phonon-Mediated Excitation Pathways in Semiconducting Single-Walled Carbon Nanotubes. *Nano Lett.* **2012**, *12*, 813−819.
(29) Kim, J.-H.; Han, K.-J.; Kim, N.-J.; Yee, K.-J.; Lim, Y.-S.; Sanders, G. D.; Stanton, C. J.; Booshehri, L. G.; Hároz, E. H.; Kono, J. Chirality-Selective Excitation of Coherent Phonons in Carbon Nanotubes by Femtosecond Optical Pulses. *Phys. Rev. Lett.* **2009**, *102*, 037402.
(30) Sanders, G. D.; Stanton, C. J.; Kim, J.-H.; Yee, K.-J.; Lim, Y.-S.; Hároz, E. H.; Booshehri, L. G.; Kono, J.; Saito, R. Resonant Coherent Phonon Spectroscopy of Single-Walled Carbon Nanotubes. *Phys. Rev. B* **2009**, *79*, 205434.

(31) Habenicht, B. F.; Prezhdo, O. V. Nonradiative Quenching of Fluorescence in a Semiconducting Carbon Nanotube: A Time-Domain *Ab Initio* Study. *Phys. Rev. Lett.* **2008**, *100*, 197402.
(32) Pollard, W. T.; Dexheimer, S. L.; Wang, W.; Peteanu, L. A.; Shank, C. V.; Mathies, R. A. Theory of Dynamic Absorption Spectroscopy of Nonstationary States. 4. Application to 12-fs Resonant Impulsive Raman Spectroscopy of Bacteriorhodopsin. *J. Phys. Chem.* **1992**, *96*, 6147−6158.
(33) Ziegler, H. J.; Vidal, J.; Cheng, T. K.; Ippen, E. P.; Dresslhaus, G.; Dresselhaus, M. Theory for Displacive Excitation of Coherent Phonons. *Phys. Rev. B* **1992**, *45*, 768−778.
(34) Engel, G. S.; Calhoun, T. R.; Read, E. L.; Ahn, T.-K.; Mančal, T.; Cheng, Y.-C.; Blankenship, R. E.; Fleming, G. R. Evidence for Wavelike Energy Transfer Through Quantum Coherence in Photosynthetic Systems. *Nature* **2007**, *446*, 782−786.
(35) Sazonova, V.; Yaish, Y.; Üstünel, H.; Roundy, D.; Arias, T. A.; McEuen, P. L. A Tunable Carbon Nanotube Electromechanical Oscillator. *Nature* **2004**, *431*, 284−287.
(36) Rabitz, H.; de Vivie-Riedle, R.; Motzkus, M.; Kompa, K. Chemistry — Whither the Future of Controlling Quantum Phenomena? *Science* **2000**, *288*, 824−828.
(37) Grumstrup, E. M.; Johnson, J. C.; Damrauer, N. H. Enhanced Triplet Formation in Polycrystalline Tetracene Films by Femtosecond Optical-Pulse Shaping. *Phys. Rev. Lett.* **2010**, *105*, 257403.
(38) Remacle, F.; Levine, R. D. An Electronic Timescale for Chemistry. *Proc. Natl. Acad. Sci. U.S.A.* **2006**, *103*, 6793−6798.
(39) Dutoi, A. D.; Cederbaum, L. S. An Excited Electron Avoiding a Positive Charge. *J. Phys. Chem. Lett.* **2011**, *2*, 2300−2303.
(40) Schneck, J. R.; Walsh, A. G.; Green, A. A.; Hersam, M. C.; Ziegler, L. D.; Swan, A. K. Electron Correlation Effects on the Femtosecond Dephasing Dynamics of E_{22} Excitons in (6,5) Carbon Nanotubes. *J. Phys. Chem. A* **2011**, *115*, 3917−3923.
(41) Koyama, T.; Miyata, Y.; Kishida, H.; Shinohara, H.; Nakamura, A. Photophysics in Single-Walled Carbon Nanotubes with (6,4) Chirality at High Excitation Densities: Bimolecular Auger Recombination and Phase-Space Filling of Excitons. *J. Phys. Chem. C* **2013**, *117*, 1974−1981.
(42) Bachilo, S. M.; Balzano, L.; Herrera, J. E.; Pompeo, F.; Resasco, D. E.; Weisman, R. B. Narrow (*n*,*m*)-Distribution of Single-Walled Carbon Nanotubes Grown Using a Solid Supported Catalyst. *J. Am. Chem. Soc.* **2003**, *125*, 11186−11187.
(43) Lüer, L.; Hoseinkhani, S.; Polli, D.; Crochet, J.; Hertel, T.; Lanzani, G. Size and Mobility of Excitons in (6,5) Carbon Nanotubes. *Nat. Phys.* **2009**, *5*, 54−58.
(44) Kataura, H.; Kumazawa, Y.; Maniwa, Y.; Umezu, I.; Suzuki, S.; Ohtsuka, Y.; Achiba, Y. Optical Properties of Single-Wall Carbon Nanotubes. *Synth. Met.* **1999**, *103*, 2555−2558.
(45) Kresse, G.; Furthmuller, J. Efficient Iterative Schemes for *Ab Initio* Total-Energy Calculations Using a Plane-Wave Basis Set. *Phys. Rev. B* **1996**, *54*, 11169−11186.
(46) Perdew, J. P.; Burke, K.; Ernzerhof, M. Generalized Gradient Approximation Made Simple. *Phys. Rev. Lett.* **1996**, *77*, 3865−3868.
(47) Blochl, P. E. Projected Augmented-Wave Method. *Phys. Rev. B* **1994**, *50*, 17953−17979.
(48) Craig, C. F.; Duncan, W. R.; Prezhdo, O. V. Trajectory Surface Hopping in Time-Dependent Kohn−Sham Approach for Electron-Nuclear Dynamics. *Phys. Rev. Lett.* **2005**, *95*, 163001.